CHEMISTRY
A EUROPEAN JOURNAL

DOI: 10.1002/chem.200800755

A New Method for the Rapid Synthesis of Water Stable Superparamagnetic Nanoparticles

Fernando Herranz,[a] M. Puerto Morales,[b] Alejandro G. Roca,[b] Manuel Desco,[c] and Jesús Ruiz-Cabello*[a]

The synthesis of water stable magnetic nanoparticles (NP) is a research topic of great interest for the past few years. These ferrofluids are used as contrast agents in magnetic resonance imaging (MRI), magnetic drug delivery, and cancer treatment through hyperthermia.[1] Particularly in the field of MRI the use of NP as contrast agents has several advantages, such as the low toxicity of the iron oxide compounds and the superparamagnetic behaviour, which lead to a greater response for the same applied field compared to paramagnetic agents.[2]

Nowadays the best method to obtain the iron oxide NP is based on high-temperature decomposition of organic precursors.[3] We have prepared monodisperse and highly crystalline NP with a mean hydrodynamic size of 7 nm (see Supporting Information), coated with oleic acid and, therefore only stable in organic non-polar solvents.[4] The major challenge in the development of NP for biomedical applications is to make them hydrophilic, stable at physiological conditions and without significant aggregation.

To implement such a modification, two different approaches are mainly used. One is the ligand exchange method in which the oleic acid is replaced, at least partially, by different hydrophilic compounds. The second methodology is based on the formation of a bilayer by the use of amphiphilic molecules, with the aim of masking the oleic acid layer. Despite the great progress made using these approaches, some major drawbacks are still present, such as low exchange ratio, irreversible desorption of new surfactants from the particle and a complicated surface modification due to the dynamic nature of the outer layer.[5]

Here we report a new route to synthesize water-dispersed superparamagnetic iron oxide (SPIO) and ultrasmall superparamagnetic iron oxide (USPIO) nanoparticles (Scheme 1).

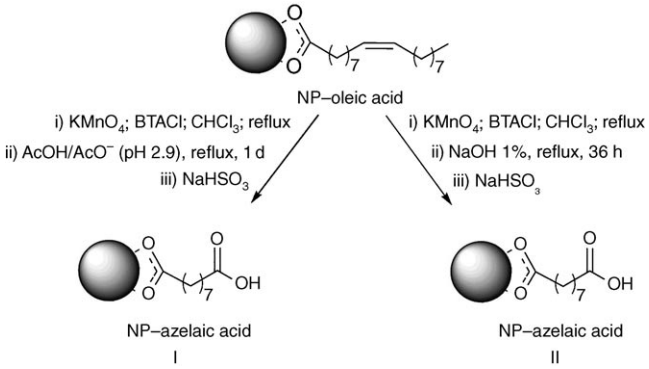

Scheme 1. New approach for the preparation of water ferrofluids.

We oxidized the double bond in oleic acid with potassium permanganate, which led to the formation of azelaic acid in the surface of the NP. The presence of this diacid on the surface of the NP leads to a great stability of the colloid because of the hydrophilic character of this functional group.

Following our proposal, water stable particles have been obtained, which show a great colloidal stability, and, more important, are ready for further functionalization by covalent bonding of bioactive molecules.

[a] Dr. F. Herranz, Dr. J. Ruiz-Cabello
Instituto de Estudios Biofuncionales
Centro de Investigación Biomédica en Red
de Enfermedades Respiratorias (CIBERES)
Universidad Complutense, Paseo Juan XXIII n° 1
28040 Madrid (Spain)
Fax: (+34) 913943245
E-mail: ruizcabe@farm.ucm.es

[b] Dr. M. P. Morales, A. G. Roca
Instituto de Ciencia de Materiales de Madrid
CSIC, Cantoblanco, 28049 Madrid (Spain)

[c] Dr. M. Desco
Unidad de Medicina y Cirugía Experimental
Hospital General Universitario Gregorio Marañón
28007 Madrid (Spain)

Supporting information for this article is available on the WWW under http://dx.doi.org/10.1002/chem.200800755.

The oxidation of the double bond is carried out by the use of a typical oxidizing reagent such as potassium permanganate. In order to obtain the required concentration of the oxidant in an organic solvent, a phase-transfer catalyst, such as benzyltrimethylammonium chloride (BTACl) was used. The final step in the oxidation method was the cleavage of an organomanganese intermediate, which formed between the permanganate ion and the double bond both in acid or basic media. For this reason, we will refer to the acid or basic oxidation in the following discussion.

Fourier transform infrared (FTIR) spectroscopy was used to characterize the composition of the NP after oxidation of the double bond. Figure 1 displays the spectra for a) NP **I** (acid method), b) NP **II** (basic method) and c) the original hydrophobic NP. The spectrum in Figure 1c shows signals corresponding to the oleic acid moiety at 2918 (ν_a C–H), 2850 (ν_s C–H) and 1411 cm^{-1} (δ_s C–H). Another sharp band is observed at 1621 cm^{-1} corresponding to the carbonyl group. Finally, the Fe–O (magnetite) stretching signal appears at $\tilde{\nu}$ 594 cm^{-1}. The spectra in Figure 1a and b correspond to the oxidized NP.

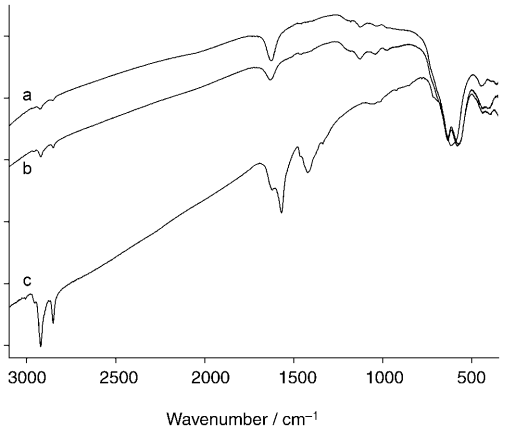

Figure 1. FTIR spectra of a) NP **I**, b) NP **II** and c) hydrophobic NP.

The formation of azelaic acid is supported by several bands. First, there are three modifications in comparison with spectrum in Figure 1c; the lack of the C–H signals due to the minor number of CH_2 groups, the broadened C=O peak at 1625 cm^{-1} due to the presence of two carbonyl groups in the molecule and the disappearance of the signal at 1567 cm^{-1} assigned to double bond in oleic acid. Regarding the structure of the carboxylate group in the surface of the NP the three samples show a difference smaller than 200 cm^{-1} between the bands at 1625 and 1460 cm^{-1}, which implies a bridging coordination for the three samples.[6,7] On the other hand, in the spectra of NP **I** and **II**, at least four bands can be clearly assigned to the azelaic acid molecule at $\tilde{\nu}$ 984, 1036, 1126 and 1192 cm^{-1}.[8] Finally, in the region between 850–250 cm^{-1}, two main absorption bands around 590 and 398 cm^{-1} assigned to magnetite are observed.

It is clear that due to the strong oxidation process used for the surface modification of the NP, a slight oxidation of the iron oxide NP from magnetite to maghemite, at least on the surface, takes place; this is indicated by the appearance of two weak bands at 634 and 445 cm^{-1}.[9] To further prove the oxidation of the double bond the organic layer of the reaction was analyzed by ^{1}H NMR spectroscopy. The chloroform and hexane mixture were evaporated in vacuum and the residue dissolved in deuterated chloroform. The signals corresponding to the nonanoic acid are clearly observable (δ 0.90 (t, 3H), 1.27 (m, 10H), 1.66 (m, 2H) and 2.38 (t, 2H) ppm). Furthermore there is no evidence of the presence of oleic acid that could be removed from the surface in the oxidation process (see Supporting Information).

The size of the hydrophilic nanoparticles, determined by photon correlation spectroscopy (PCS) are 37 ± 4 nm (PDI 0.18) for NP **I** (USPIO) and 70 ± 7 nm (PDI 0.25) for NP **II** (SPIO). The data shown here correspond to the *z*-average value as measured by PCS. The *z*-average size is the most important and stable number produced by this technique for characterizing the hydrodynamic diameter of nanoparticles in solution. This is the number required for quality control purposes. PCS values can be obtained in a *z*-average size, or the mean value of a distribution by intensity, volume or number. In order to obtain meaningful results these values must be similar. For the particles studied in our work, all PCS measurements show great reproducibility and excellent correlation between the different methods with which the values were obtained. For example, the values for one of the samples obtained with the oxidation in acid media are: *z*-average = 39 nm, intensity = 43 nm, volume = 27 nm and number (size) = 21 nm.

The differences in size between the two oxidation protocols could be attributed to the considerable oxidation capacity of permanganate in acid media, allowing the use of a lower concentration of the oxidant and the phase-transfer catalyst. There is a small increase in the size of the NP from the hydrophobic state to the water colloid. This degree of aggregation and broadening of the size distribution of the aggregates is unavoidable but can be drastically reduced by using the method described in this work as can be seen from the PDI values. By the method proposed here, particle aggregation is minimum compared with previous reported methods. One big advantage is that the particles are ready for functionalization through covalent bonding in water. These nanoparticles show high stability in water and no aggregation with time, as can be seen in Figure 2 where the *z*-average value is plotted versus time.

Another important feature of the NP regarding their stability in water is the ζ potential. This value was determined by PCS; the results are shown in Figure 3. A similar profile is obtained with both methods, but the stability for NP **I** is higher (−46 mV) than for NP **II** (−20 mV) at physiological pH. This can be attributed to the slightly higher agglomeration of NP **II** compared with NP **I**, which leads to a smaller number of carboxylic acids on the surface. These reactions have been repeated at least 10 times and all samples showed

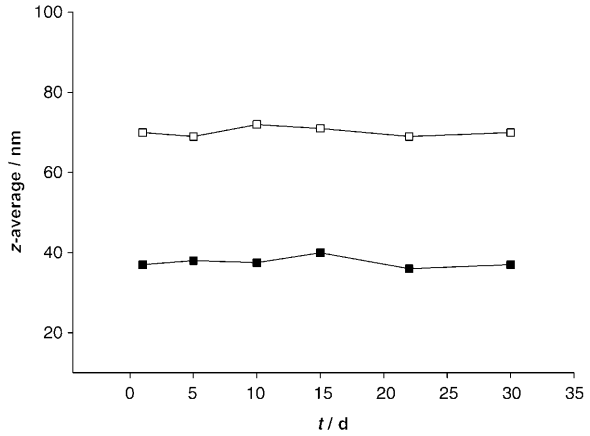

Figure 2. Hydrodynamic size evolution with time for NP **I** (■) and **II** (□).

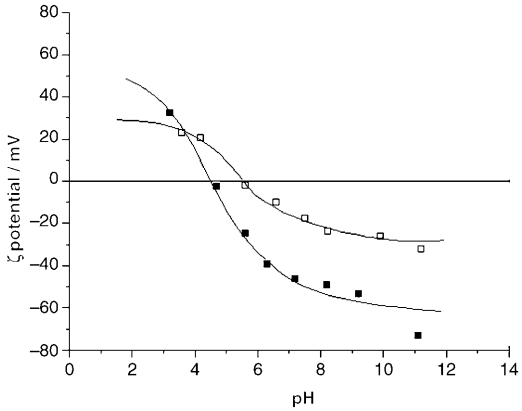

Figure 3. Profile of the ζ potential versus pH for the oxidized particles, NP **I** (■) and **II** (□).

similar hydrodynamic size, within the error and similar ζ profile; this confirms the great control over the size and the surface composition with just minor changes in the reaction.

Moreover, suspensions prepared by both methods, both in acid and basic media, remained stable in water for months. Furthermore, the ζ potential results confirm the conclusions obtained from the FTIR and NMR analysis, as the isoelectric point for these particles is approximately 4.5 for NP **I** and 5.7 for NP **II**. These results are in accordance with the pK_a values for azelaic acid which are 4.53 and 5.33, supporting the presence of the diacid in the surface of the NP.

Transmission electron microscopy (TEM) images were obtained for the three types of nanoparticles studied in this work before surface modification and after oxidation. Figure 4 shows the low aggregation which occurred during the transition of the NP from the hydrophobic state (Figure 4a) to water (NP **I**, Figure 4b and c) at the same magnification (Figure 4a and b) and at larger one (Figure 4c).

Although the oxidized particles are not self-assembled as the hydrophobic ones, a certain distance between particles can be observed which precludes the aggregation and formation of big lumps (for more TEM images, see Supporting Information).

To study the magnetic properties of the suspensions, magnetization curves were performed for the hydrophobic NP in hexane and both NP **I** and NP **II** (Figure 5). The three samples show a superparamagnetic behavior with saturation magnetization values of 87 emu g^{-1} Fe for hydrophobic NP, 77 emu g^{-1} Fe for NP **I** and 63 emu g^{-1} Fe for NP **II**. The expected value for bulk magnetite at room temperature would be 110 emu g^{-1} Fe; this means that particles prepared in this work have a certain degree of surface oxidation (as confirmed by FTIR spectra) which increases from the hydrophobic to hydrophilic samples.

The different susceptibility at low field can be related to the size of the aggregate in the suspension in such a way, that greater susceptibility corresponds to sample NP **II** with a larger aggregate size. These results are in agreement with the hydrodynamic sizes measured by PCS.

Finally, to test the behavior of this hydrophilic NP as contrast agents for MRI, we measured the longitudinal (T_1) and transversal (T_2) relaxation times (Figure 6). For NP **I** the values for r_1 and r_2 are 4 s^{-1} mM^{-1} and 115 s^{-1} mM^{-1}, while for NP **II** the values are 2.3 s^{-1} mM^{-1} and 110 s^{-1} mM^{-1}, respectively. Because of the high r_1 value, mainly for NP **I**, these particles can be used either as T_1 or T_2 agents depending on the imaging sequences and parameters chosen.

We have developed a new general approach for transferring oleic acid coated nanoparticles into water. Compared to other common methodologies, the one presented here has several advantages: First, particles with mean hydrodynamic sizes of 37 and 70 nm are obtained, with a high reproducibility; previously it has been rather difficult to particles in this critical range of 30–80 nm. Second, the process described here is much more economical than approaches which use very expensive surfactants such as phospholipids. And third,

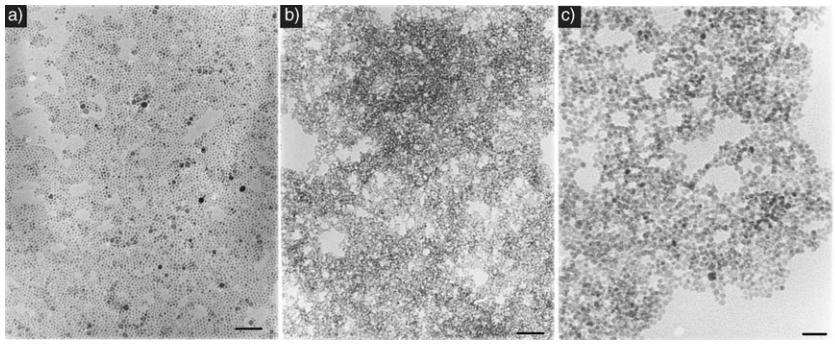

Figure 4. TEM images of iron oxide nanocrystals a) hydrophobic NP, scale bar is 50 nm; b) and c) hydrophilic NP via acid oxidation (NP **I**), scale bars are 50 and 20 nm, respectively.

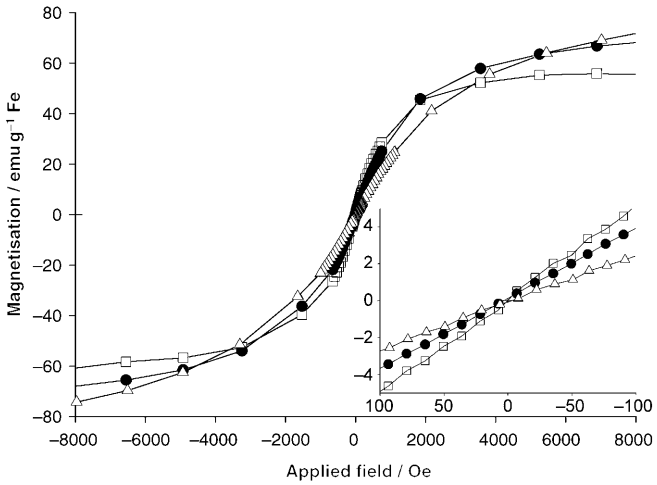

Figure 5. Main panel: magnetization curves at 298 K for hydrophobic NP (Δ), NP **I** (●) and NP **II** (□). Inset: enlargement of the magnetization curves between −100 and 100 Oe.

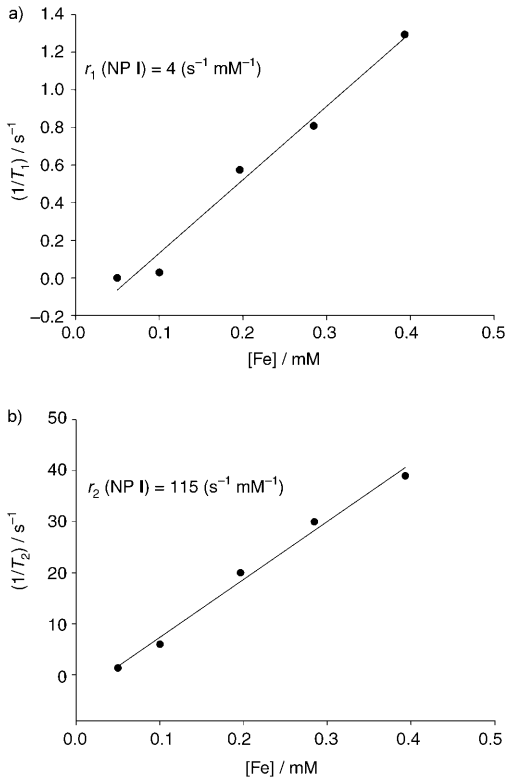

Figure 6. Plot of the relaxation rate a) T_1 and b) T_2 against iron concentration for NP **I**.

further surface functionalization of these particles is possible through covalent bonding in water; this would render the particles even more stable compared with other particles obtained by other approaches. This application is currently under investigation. Thus, we believe that this new methodology can be used as a new standard for transferring oleic acid nanoparticles into water, so that this approach will be of a great interest for those working in the development of new bioactive materials.

Experimental Section

Synthesis of hydrophobic NP: The nanoparticles were synthesized by using iron acetylacetonate as precursor and phenyl ether as the solvent. A mixture of $Fe(acac)_3$ (0.71 g, 2 mmol), 1,2-hexadecanediol (2.38 g, 10 mmol), oleic acid (1.69 g, 6 mmol), oleylamine (1.60 g, 6 mmol) and phenyl ether (20 mL) were added to a three-neck flask. Then, the reaction mixture was heated under mechanical stirring and a flow of nitrogen gas until a temperature of 200 °C was reached. This temperature was kept for 120 min and then the solution was heated to reflux (254 °C) for 30 min under nitrogen. Subsequently, the solution was cooled to room temperature. To remove the side products, ethanol was added to the reaction mixture and the resulting solution was centrifuged at 8500 rpm for 10 min. The supernatant was decanted; hexane (20 mL) and oleic acid (0.05 mL) were added to the nanoparticles and the suspension was centrifuged at 8500 rpm in order to remove aggregates and to obtain a stable suspension.

Synthesis of NP I (oxidation in acid conditions): $KMnO_4$ (0.3 g, 1.9 mmol) and benzyltrimethylammonium chloride (BTACl) (0.8 g, 4.3 mmol) were dissolved in chloroform (60 mL). This solution was added to a concentrate dispersion of NPs coated with oleic acid in hexane/chloroform (20 mL/20 mL); then the solution was mechanically stirred and heated under reflux for 4 h. After this time, an $AcOH/AcO^-$ buffer (50 mL, pH 2.9) wass added and the mechanical stirring and heating was continued for 20 h. After cooling $NaHSO_3$ (3×2 mL) was added to eliminate excess of permanganate. Finally, the dispersion was washed several times with water and chloroform to obtain a colloidal dispersion.

Synthesis of NP II (oxidation in basic conditions): $KMnO_4$ (0.5 g, 3.2 mmol) was dissolved in chloroform (40 mL), together with BTACl (1 g, 5.4 mmol). The solution was added to a concentrate dispersion of NP coated with oleic acid in hexane/chloroform (20 mL/20 mL). The mixture was heated under reflux and mechanically stirred for 4 h; then NaOH (1 %, 20 mL) solution was added under heating and stirring for another 32 h. After cooling, $NaHSO_3$ was added (3×2 mL) to eliminate the excess of permanganate. Finally the dispersion was washed several times with water and chloroform to obtain a colloidal dispersion.

Relaxometry: All images were acquired in a Bruker Biospec spectrometer (Bruker Biospec 47/40, Bruker Biospin, Germany) equipped with an 11.2 cm gradient probe capable of producing gradients of up to 200 $mT\,m^{-1}$. Images to obtain a T_2 parametric map were acquired using a normal spin echo sequence consisting of 90° pulse and a train of equally spaced 180 pulses with switching phases (Carr–Purcell–Meiboom–Gill–Hill pulse sequence). Images were acquired with 20 TEs (6–120 ms) and with a TR of 5 s. Other imaging parameters included 100 kHz spectral width, 6 cm square field of vision, 2 mm slice thickness, and 64×64 acquisition matrix size. A T_1 parametric map was extracted from saturation recovery imaging data using a single spin echo sequence with the shortest TE for our equipment and sequence parameters (6 ms) and variable TR from 50 to 3000 ms, tailored to provide sampling times with adequate coverage of the T_1 recovery curve. Other imaging parameters included were identical to T_2 acquisitions. Both T_1 and T_2 values were obtained from nonlinear least squares fitting routines included in commercial software (Bruker Paravision 3.0, Bruker Biospin, Germany).

Magnetic measurements: Magnetic characterization of the samples was carried out in a vibrating sample magnetometer using 100 μL of solution in a special sample holder. Magnetization curves were recorded at room temperature by first saturating the sample in a field of 1 T. The magnetization values were normalized to the amount of iron to yield the specific magnetization ($emu\,g^{-1}$ Fe). The initial susceptibility (χ) of the suspensions was measured in the field range ±100 Oe and the saturation magnetization values (M_s) were evaluated by extrapolating to infinite field the experimental results obtained in the high field range where the magnetization linearly increases with 1/H.

Acknowledgements

This work has been carried out under financial support of MEC (NAN2004-08805-C04-01 and SAF2008-05412) and Madrid regional government CAM (S0505-AGR-0187). Dr. Sabino Veintemillas is gratefully acknowledged for helpful comments and suggestions.

Keywords: colloids · contrast agents · magnetic properties · molecular imaging · nanostructures

[1] a) S. Benderbous, C. Corot, P. Jacobs, B. Bonnemain, *Acad. Radiol.* **1996**, *3*, S292–S294; b) Q. A. Pankhurst, *BT Technology J.* **2006**, *24*, 33–38; c) P. Tartaj, M. P. Morales, S. Veintemillas-Verdaguer, T. González-Carreño, C. J. Serna, *J. Phys. D* **2003**, *36*, R182–R197.

[2] a) S. Pérez-Rial, I. Rodríguez, J. González, J. Pérez-Sánchez, F. Herranz, N. Beckmann, J. Ruíz-Cabello, *J. Pharm. Sci.* **2008**, 3637–3665; b) C. J. Sunderland, M. Steiert, J. E. Talmadge, A. M. Derfus, S. E. Barry, *Drug Dev. Res.* **2006**, *67*, 70–93.

[3] a) T. Hyeon, S. L. Su, J. Park, Y. Chung, B. N. Hyon, *J. Am. Chem. Soc.* **2001**, *123*, 12798–12801; b) J. Rockenberger, E. C. Scher, A. P. Alivisatos, *J. Am. Chem. Soc.* **1999**, *121*, 11595–11596; c) W. W. Yu, J. C. Falkner, C. T. Yavuz, V. L. Colvin, *Chem. Commun.* **2004**, 2306–2307.

[4] A. G. Roca, M. P. Morales, K. O'Grady, C. J. Serna, *Nanotechnology* **2006**, *17*, 2783–2788.

[5] a) M. Lattuada, T. A. Hatton, *Langmuir* **2007**, *23*, 2158–2168; b) T. Pellegrino, L. Manna, S. Kudera, T. Liedl, D. Koktysh, A. L. Rogach, S. Keller, J. Radler, G. Natile, W. J. Parak, *Nano Lett.* **2004**, *4*, 703–707; c) E. Taboada, E. Rodriguez, A. Roig, J. Oro, A. Roch, R. N. Muller, *Langmuir* **2007**, *23*, 4583–4588; d) T. R. Zhang, J. P. Ge, Y. P. Hu, Y. D. Yin, *Nano Lett.* **2007**, *7*, 3203–3207.

[6] L. M. Bronstein, X. Huang, J. Retrum, A. Schmucker, M. Pink, B. D. Stein, B. Dragnea, *Chem. Mater.* **2007**, *19*, 3624–3632.

[7] A. C. S. Anna C. S. Samia, J. A. Schlueter, J. S. Jiang, S. D. Bader, C.-J. Qin, X.-M. Lin, *Chem. Mater.* **2006**, *18*, 5203–5212.

[8] H. M. Hung, P. Ariya, *J. Phys. Chem. A* **2007**, *111*, 620–632; H. M. Hung, Y. Katrib, S. T. Martin, *J. Phys. Chem. A* **2005**, *109*, 4517–4530.

[9] A. G. Roca, M. P. Morales, C. J. Serna, *IEEE Trans. Magn.* **2006**, *42*, 3025–3029.

Received: April 21, 2008
Published online: September 12, 2008

